A Reproduced Copy

OF

Reproduced for NASA

by the

NASA Scientific and Technical Information Facility

TECHNICAL NOTE SE-292

TECHNICAL NOTE SE-292

A STUDY OF SPALLATION RESULTING FROM HYPERVELOCITY IMPACT-GENERATED WAVES

by T. S. Fu

April 1970

SCIENCE & ENGINEERING

BROWN ENGINEERING

Research Park • Huntsville, Alabama 35807

TECHNICAL NOTE
SE-292

A STUDY OF SPALLATION RESULTING FROM HYPERVELOCITY IMPACT-GENERATED WAVES

By

T. S. Fu, Ph. D.

April 1970

Prepared For

SPACE SCIENCES LABORATORY
GEORGE C. MARSHALL SPACE FLIGHT CENTER
HUNTSVILLE, ALABAMA

Contract No. NAS8-20166

Prepared By

SPACE AND MILITARY SYSTEMS DIVISION
SCIENCE AND ENGINEERING GROUP
BROWN ENGINEERING COMPANY, INC.
HUNTSVILLE, ALABAMA

ABSTRACT

This report presents a study of spallation produced by the reflected stress wave due to hypervelocity impact. Emphasis is placed on the matching of the solutions in hydrodynamic and elastic regimes. Hydrodynamic shock solutions are utilized as the initial condition for the elastic wave pattern.

A sample calculation of the spall fracture is made in this study. Even though no direct comparison with experiments is possible, the qualitative features are compatible with available experimental observations.

Approved:

G. R. Guinn

G. R. Guinn, Ph. D.
Manager
Thermal Systems Branch

Approved:

J. E. White, Jr.

J. E. White, Jr.
Program Manager
Science and Engineering Group

Approved:

R C Watson

R. C. Watson, Jr.
Vice President
Science and Engineering Group

TABLE OF CONTENTS

LIST OF ILLUSTRATIONS

LIST OF SYMBOLS

c	Dilatational wave speed
F, G	Solutions of wave equation
f, g	Defined in Equation 15
p, q	Principal stresses
R	Radius of elastic wave
R_s	"Equivalent" spherical wave radius (Equation 8)
R_w	Radius of elastic wave in image system
r	Radial coordinate
t	Time
u	Displacement function
v	Velocity function
v_0	Initial velocity distribution
v_1	Hugoniot velocity
z	Axial coordinates
z_i	$2R_s - z$ (see Figure 7)
λ, μ	Lame's constants of elasticity
ξ	Defined in Equation 12
ρ	Density
σ	Normal stresses
γ	Angle between r axis and maximum principal stress
τ	Shear stresses
ϕ	Displacement potential

INTRODUCTION

The impact of a projectile on a target at hypervelocity drives strong compressive waves into the target. When such waves encounter a free surface, they are reflected as tensile stress waves. A fracture may occur near the free surface if the tensile stress or the amplitude of the reflected waves exceed the dynamic stress of the target material. The fracture formation caused by the reflected stress waves is called spallation, or spall fracture.

A precise treatment of the problem is difficult because the compressive wave attenuates through different stress regimes, i.e., hydrodynamic, plastic, and elastic, as the wave advanced into the target. The behavior of a compressive wave in each regime is governed by different systems of equations. In the early stage of impact the pressures are considerably above the material strength, thus the compressive wave may be described by the shock wave theory of an inviscid, compressible fluid*. Thereafter, the shock strength decays to a point where the effects of solid material strength become important and the theory of plasticity, or ultimately elasticity, applies.

Spallation has been studied by a number of investigators, and several approaches have been proposed. A comprehensive review of spall fracture has been made by Rae (Ref. 1) in which various approaches were discussed in detail.

The approach presented in this report is to use the hydrodynamic shock solutions described in Reference 2, up to the point where the incident waves first reach the free surface, and then to use the elastic wave theory for the wave interaction resulting from the wave reflections.

*The attenuation and the distortion of a two-dimensional, impact-generated shock wave in a target are discussed in Reference 2.

Because the shock wave develops into a spherical shape very rapidly as it propagates into the target, the assumption of spherical incident wave is made in the present analysis.

The problems of propagation and reflection of a spherical elastic wave from a free boundary have been investigated by Aliev (Ref. 3), Rinehart (Ref. 4), Kinslow (Refs. 5, 6, and 7), and others. The basic approach relative to the wave reflection is to use a simple image system by which the zero stress condition on the free surface is obtained. A detailed discussion on various images can be found in References 1 and 7. The present investigation also uses the idea of image, but the image system employed in this report differs slightly from those proposed by other authors.

In most theoretical spallation studies, the pressure pulse of the incident wave is imposed in a rather arbitrary way (Refs. 8 and 9). However, the shape of the pressure pulse is a decisive factor in establishing location of the spall fracture relative to the free surface. The essential feature of the present analysis is the use of the "realistic" hypervelocity shock profiles from Reference 2 as an input to the elastic wave reflection.

The author wishes to express his appreciation to Mr. C. T. Young for his discussions of the problem and to Dr. G. R. Guinn for his guidance and encouragement during the course of this work.

IMPACT-GENERATED SHOCK WAVES

Since shock wave profiles generated by the methods of Reference 2 will be used as an input of the incident wave for the spall prediction, a brief description of shock wave characteristics is given in this section. Details of shock wave propagation and related topics are reported in Reference 2.

DYNAMICS OF TARGET SHOCK WAVES

The features of shock wave propagation resulting from hypervelocity impact are illustrated schematically in Figure 1. When a hypervelocity projectile strikes a target, shock waves are generated immediately after impact (Figure 1a). The target shock, which starts as a plane form, gradually distorts its shape into a spherical form and also attenuates in strength as it propagates into the target (Figure 1b). After an extended elapsed period following impact, a crater is formed in the target, while the isolated shock wave continues to propagate into the target (Figure 1c). Further advancement into the target will cause the shock wave to degenerate into plastic waves and then into elastic waves through dissipative effects.

Figure 1 shows the shock wave propagation in a semi-infinite target. For a target of finite thickness, i.e., a flat target plate, the shock wave will be reflected from the rear surface and becomes a rarefaction wave. The spall fractures will occur near the rear surface if the strength of the reflection wave exceeds the material strength of the target.

SHOCK WAVE SOLUTIONS

The solutions of a two-dimensional and axis-symmetric shock wave propagation are given in Reference 2 based on a shock diffraction theory in fluid mechanics. A numerical example of aluminum impacting

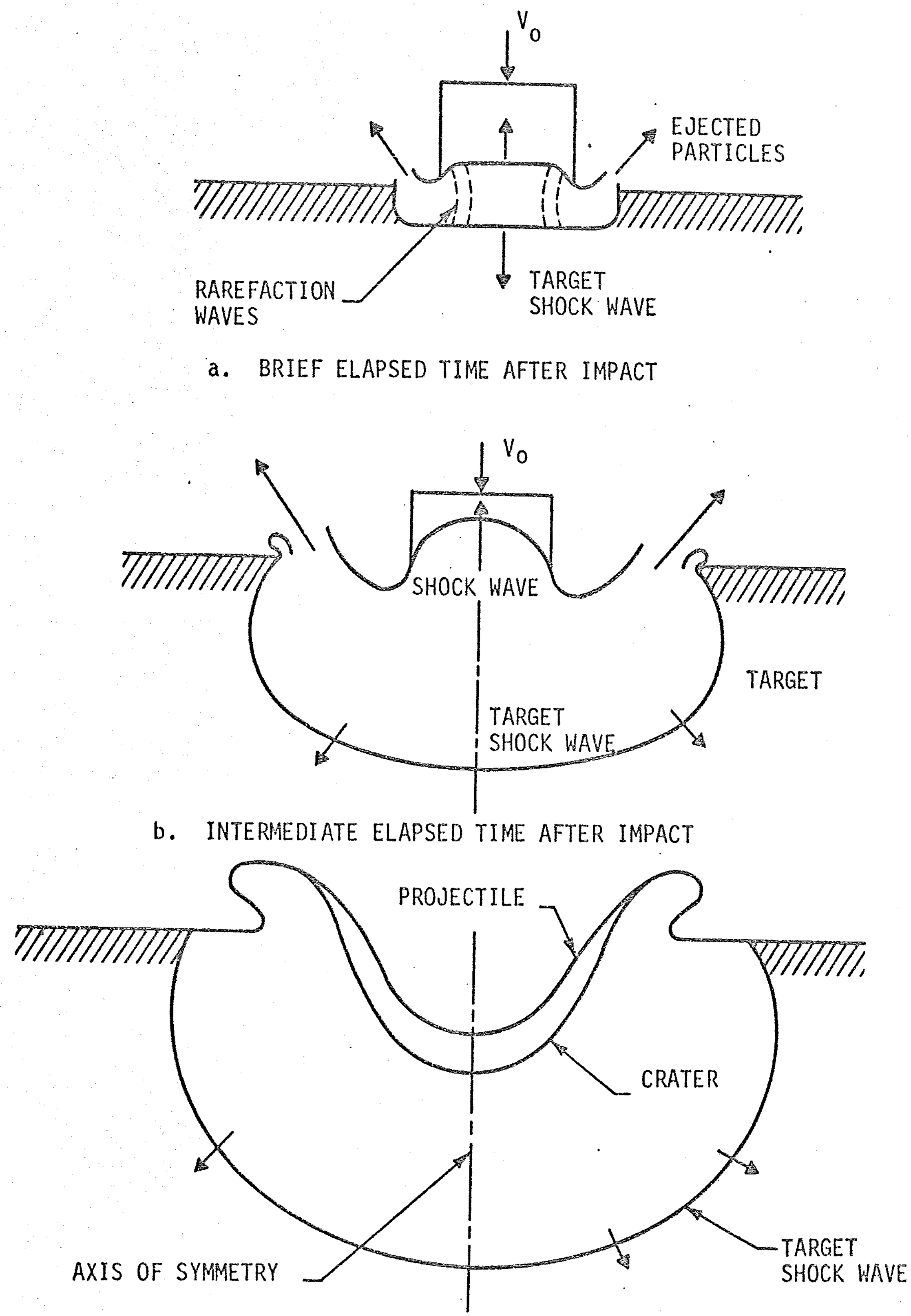

a. BRIEF ELAPSED TIME AFTER IMPACT

b. INTERMEDIATE ELAPSED TIME AFTER IMPACT

c. EXTENDED PERIOD OF TIME AFTER IMPACT

FIGURE 1. GENERAL FEATURES OF THE HYPERVELOCITY IMPACT MECHANISM

on aluminum at a velocity of 20 km/sec was obtained by the method of characteristics. Figure 2 presents the positions of shock profiles as functions of successive steps. The normal shock portion vanishes very rapidly and it completely disappears at about 5.5 microseconds. The shock profile develops further into an ellipsoid and eventually approaches a hemispherical shape. A comparison with the direct numerical solution obtained from Reference 10 is made in Figure 3, and the agreement, in general, is good.

The appearnace of the hemispherical shock shape supports the assumption of spherical symmetry in this study. This approximation, as in the case of the strip theory in hypersonic flow (Ref. 11), permits reduction of the independent variable in the governing equation.

By the approximation of spherical symmetry, the flow properties in the shocked region are obtained using the quasi-similarity solutions of the blast wave theory (Ref. 2). These solutions will be used in the present study to establish the incident wave characteristics.

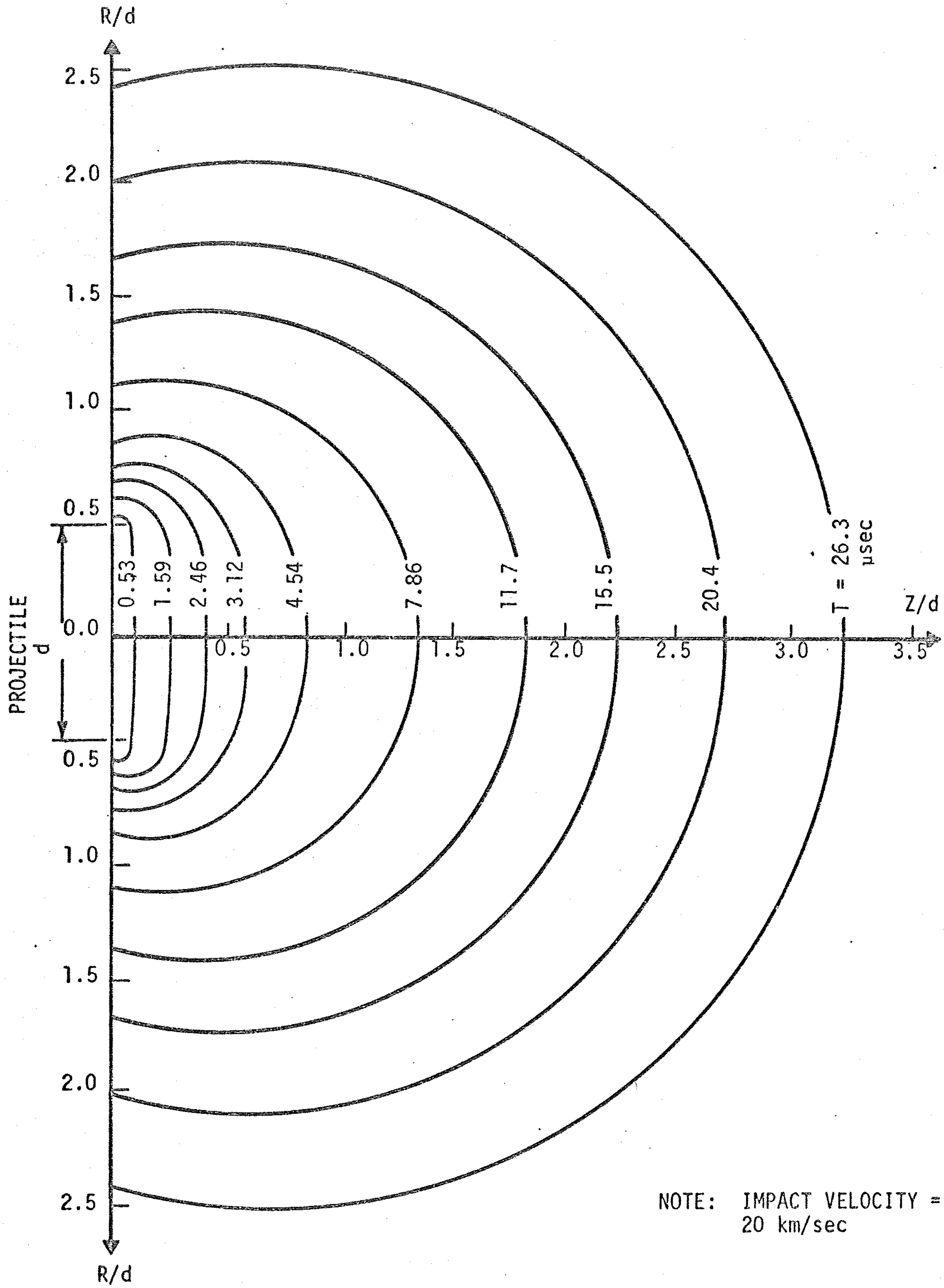

FIGURE 2. SUCCESSIVE SHOCK PROFILES FOR ALUMINUM-ON-ALUMINUM IMPACT

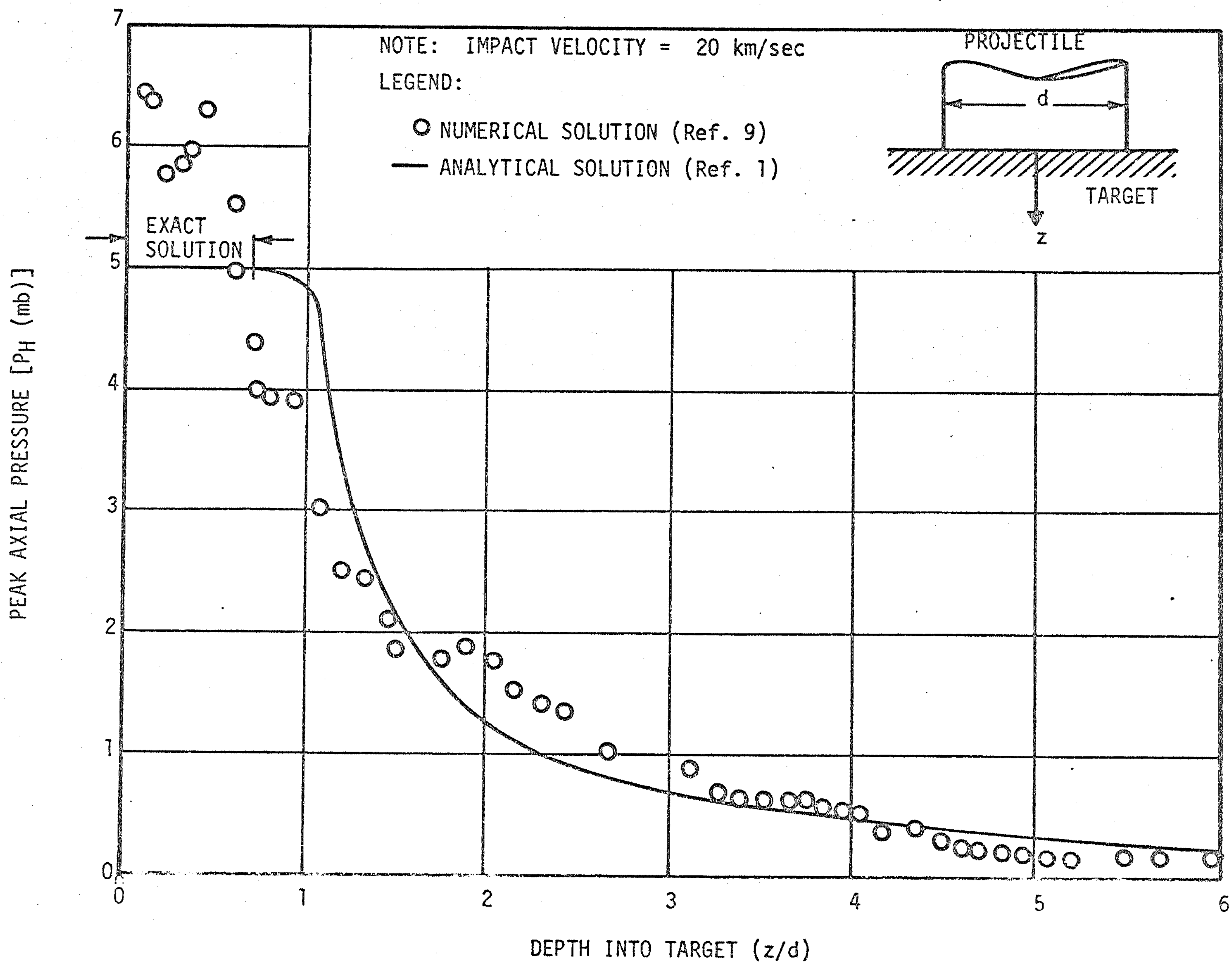

FIGURE 3. COMPARISON OF PEAK PRESSURE DISTRIBUTION FOR ALUMINUM-ON-ALUMINUM IMPACT

ELASTIC WAVE MODEL

As mentioned previously, the shock waves may decay into plastic waves and then into elastic waves at the late stage of wave propagation into the target. For simplicity, an approximation is made that the target material response is assumed to become elastic at the instant the incident wave reaches the target-free boundary. Moreover, an incident spherical wave is assumed, and the incident shear stress wave is considered to have no effect on spallation because of small angular variation of the pressure (stresses) distribution on the incident wave (Figures 2 and 4).

From the elastic wave theory, it is known that as a stress wave strikes the target rear surface it reflects into a wave of opposite sense because of the requirement of zero stress on the free boundary. Hence, a compressive stress wave should be reflected as a tensile wave, and, conversely, a tensile wave should be reflected as a compressive wave.

Since spall fracture is related to tensile stress, some features of the mechanism can be obtained by considering stress wave reflections normal to the free boundary (Figure 5). In order to statisfy the zero stress condition on the free surface, an inverted image of the incident wave and an externally applied shear stress distribution are assumed, as shown in Figure 6. The principal stress, after the wave reflection, can be calculated as the vectorial sum of these three systems, i.e., the incident, the image, and the externally applied shear stresses. When the reflected principal stress exceeds the dynamic fracture strength of the material, the spall fracture occurs near the free surface of the target.

The present approximation is simpler than the one proposed by Kinslow (Ref. 7) who utilizes a moving cavity to balance the shear stress on the free surface. However, the present approach may produce more accurate results than those models in which the shear stress on free stress is ignored (Refs. 3 and 5).

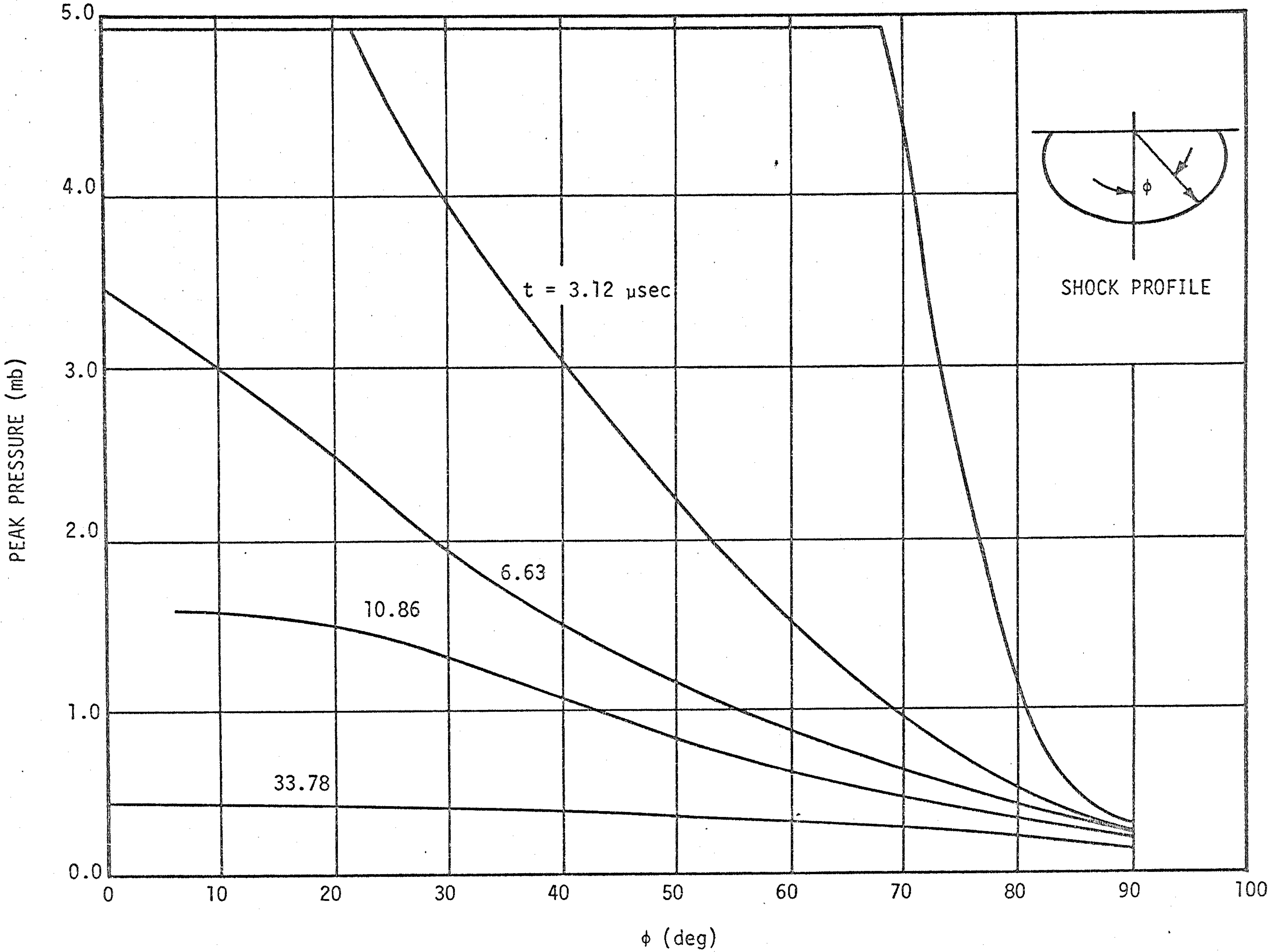

FIGURE 4. ANGULAR PRESSURE DISTRIBUTION

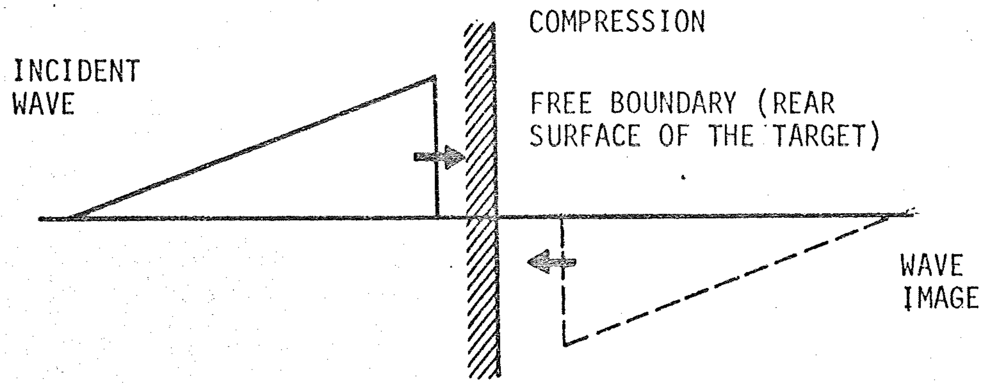

a. AN INCIDENT WAVE MOVES TOWARD A FREE BOUNDARY

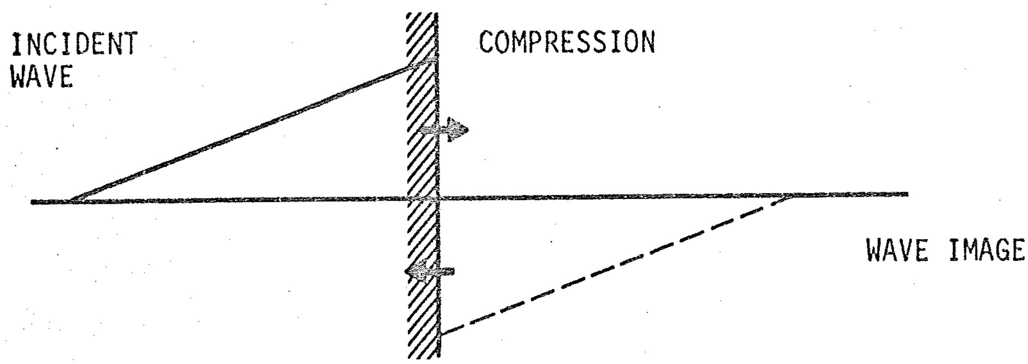

b. THE INCIDENT WAVE IS ABOUT TO REFLECT FROM THE FREE BOUNDARY

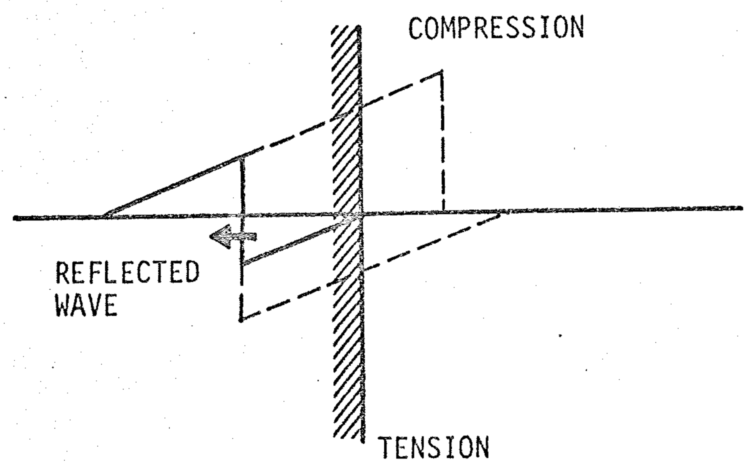

c. THE COMPRESSION WAVE IS BEING REFLECTED AS A TENSILE STRESS WAVE

FIGURE 5. COMPRESSION WAVE REFLECTION FROM A FREE BOUNDARY

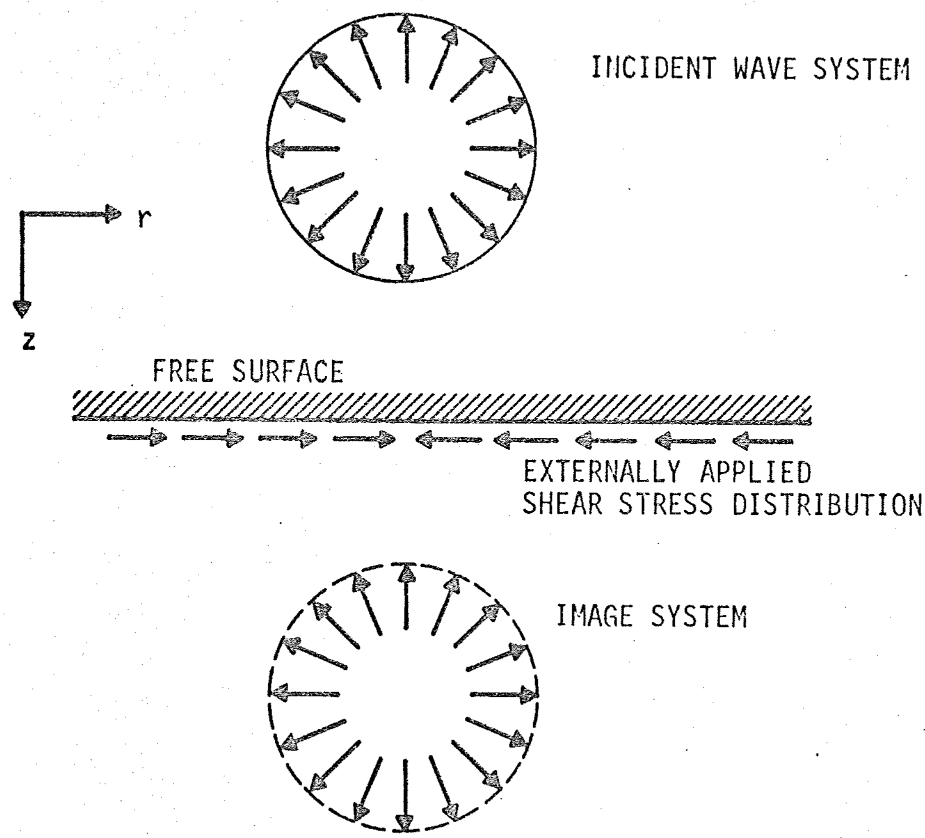

FIGURE 6. IMAGE SYSTEM AND EXTERNALLY APPLIED SHEAR STRESS DISTRIBUTION

MATHEMATICAL FORMULATION OF LINEAR ELASTIC WAVES

The governing equation of elastic wave motion in a homogeneous isotropic material can be written in the form

$$\frac{\partial^2 \phi}{\partial t^2} = c^2 \nabla^2 \phi \tag{1}$$

where

ϕ - displacement potential

t - time

∇^2 - Laplacian differential operator

c - propagation speed of a dilatational wave.

Expressing c in terms of Lame's constants λ, μ, and the material density, ρ, gives

$$c = \left(\frac{\lambda + 2\mu}{\rho}\right)^{\frac{1}{2}} . \tag{2}$$

For the case of spherical symmetry, Equation 1 becomes

$$\frac{\partial^2 \phi}{\partial t^2} = c^2 \left(\frac{\partial^2 \phi}{\partial R^2} + \frac{2}{R} \cdot \frac{\partial \phi}{\partial R}\right) \tag{3}$$

where $R = (r^2 + z^2)^{\frac{1}{2}}$ is the radius of cavity to the point of interest.

From the fundamental theory of partial differential equations, the solution of a wave equation in spherical symmetry is in the form

$$\phi = \frac{1}{R} \left[F\,(R - c\,t) + G\,(R - c\,t) \right] \tag{4}$$

where F, G are arbitrary functions, depending upon the initial conditions. F corresponds to a spherical wave diverging from the origin and G corresponds to a converging spherical wave. The amplitude in both cases is inversely proportional to the distance, R.

It is observed that only the diverging wave solution, F, is meaningful in the present problem; hence, the displacement function, u_R, and the particle velocity function, v_R, are

$$u_R = \frac{\partial \phi}{\partial R} = -\frac{F}{R^2} + \frac{F'}{R} \tag{5}$$

and

$$v_R = \frac{\partial u}{\partial t} = \frac{c\,F'}{R^2} - \frac{c\,F''}{R} \quad . \tag{6}$$

The stress functions can be expressed in terms of u_R and v_R as

$$\begin{aligned} \sigma_R &= (\lambda + 2\mu)\,\frac{\partial u_R}{\partial R} + 2\lambda\,\frac{u_R}{R} \\ \sigma_\theta &= \lambda\left(\frac{\partial u_R}{\partial R}\right) + 2\,(\lambda + \mu)\left(\frac{u_R}{R}\right) \quad . \end{aligned} \tag{7}$$

INCIDENT WAVE SOLUTION

The function, F, in Equation 6 can be determined by the initial velocity distribution, v_0 (R). In Reference 2, v_0 (R) is obtained from shock solutions, which is

$$v_0 = \frac{R}{R_s} v_1 \qquad (8)$$

where

R_s - "equivalent" spherical wave radius (Figure 7a)

v_1 - particle velocity immediately behind the shock wave.

Combining Equations 6 and 7 yields a differential equation,

$$F''(R) - \frac{F'(R)}{R} = \frac{R^2}{c\ R_s} v_1 \quad . \qquad (9)$$

The solution of Equation 9 is

$$F(R) = -\frac{v_1\ R^4}{8\ R_s\ c} \quad . \qquad (10)$$

Thus, the solution of the wave equation for time, t, is

$$\phi = F(\xi)/R \qquad (11)$$

where

$$F(\xi) = -\frac{v_1}{8\ R_s\ c}\xi^4 \quad \text{for } \xi < R_s$$

$$= 0 \quad \text{for } \xi > R_s \qquad (12)$$

and

$$\xi = R - c\ t \quad .$$

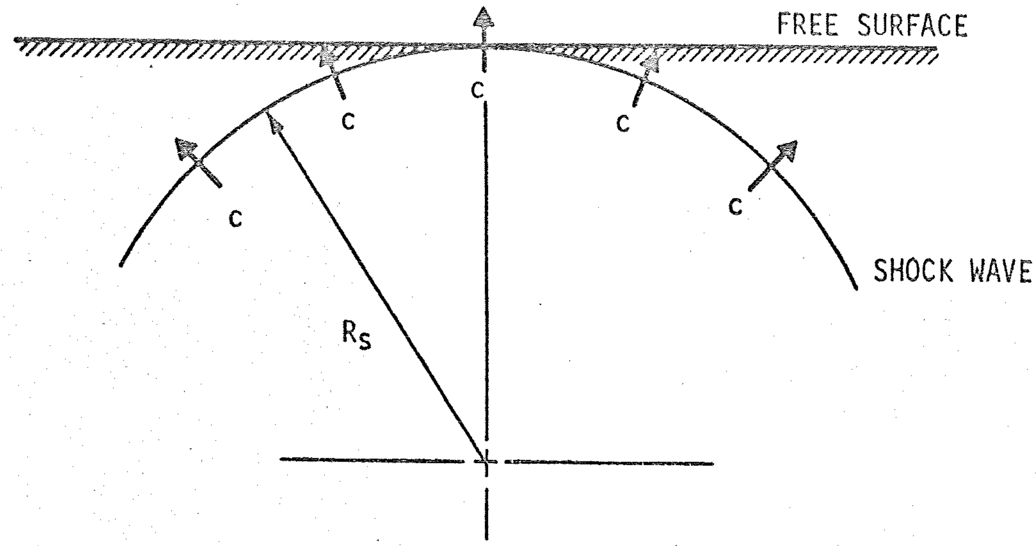

a. INITIAL SPHERICAL WAVE (SHOCK WAVE) REACHES THE FREE SURFACE AT THE TIME, t = 0

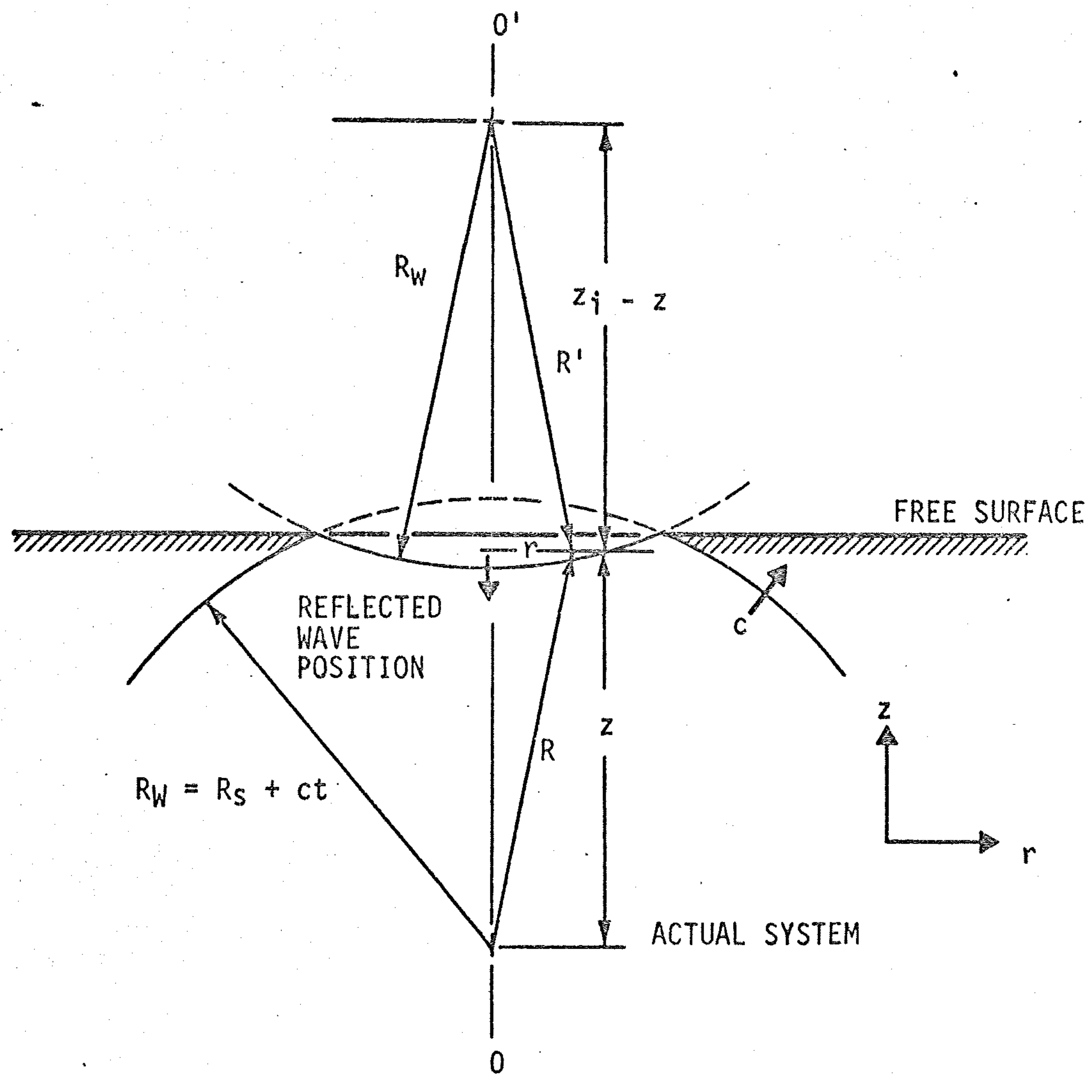

b. REFLECTION OF ELASTIC WAVE FROM FREE SURFACE

FIGURE 7. WAVE REFLECTION MODEL

REFLECTED WAVE SOLUTIONS

As shown in Figure 7b, an image system is established to determine the solutions of the reflected elastic wave. Since the boundary is free from stress, the image system, 0', is located symmetrically with respect to the free boundary. After the reflection, the motion which was spherically symmetric becomes axially symmetric.

Referring to Figure 7b,

$$\vec{R} = r\,\hat{i} + z\,\hat{j}$$
$$\vec{R}_1 = r\,\hat{i} + (z - z_i)\,\hat{j} \tag{13}$$

where $z_i = 2\,R_s$ is the distance between the actual and the image system; and $\hat{i}$ and $\hat{j}$ are unit vectors of the cylindrical coordinates, r and z.

The displacement function, $\vec{u}$, is

$$\vec{u} = (f + g)\,r\,\hat{i} + [\,(f + g)\,z - g\,z_i]\,\hat{j}$$
$$= u_r\,\hat{i} + u_z\,\hat{j} \tag{14}$$

where

$$f = -\frac{F}{R^3} + \frac{F'}{R^2}$$

$$g = -\frac{F_1}{R_1^3} + \frac{F_1'}{R_1^2}$$

$$F = F(\xi)$$

$$F_1 = F(\xi_1)$$
$$\xi_1 = R_1 - c\,t \qquad (15)$$

and prime denotes the derivative of function F.

Now, the gradients of displacement can be expressed as

$$\frac{\partial u_r}{\partial r} = (f + g) + r\left(\frac{\partial f}{\partial r} + \frac{\partial g}{\partial r}\right)$$

$$\frac{\partial u_z}{\partial r} = \left(\frac{\partial f}{\partial r} + \frac{\partial g}{\partial r}\right) z - z_i \frac{\partial g}{\partial r}$$

$$\frac{\partial u_r}{\partial z} = r\left(\frac{\partial f}{\partial z} + \frac{\partial g}{\partial z}\right) \qquad (16)$$

$$\frac{\partial u_z}{\partial z} = f + g + z\left(\frac{\partial f}{\partial g} + \frac{\partial g}{\partial z}\right) - z_i \frac{\partial g}{\partial z}$$

and the velocity function is

$$\vec{v} = v_r \hat{i} + v_z \hat{j} = \frac{\partial u_r}{\partial t} \hat{j} + \frac{\partial u_z}{\partial t} \hat{j}$$

where

$$\frac{\partial f}{\partial r} = \frac{r}{R}\left(\frac{3F}{R^4} - \frac{3F'}{R^3} + \frac{F''}{R^2}\right)$$

$$\frac{\partial f}{\partial z} = \frac{z}{R}\left(\frac{3F}{R^4} - \frac{3F'}{R^3} + \frac{F''}{R^2}\right) \qquad (17)$$

$$\frac{\partial g}{\partial r} = \frac{r}{R_1}\left(\frac{3F_1}{R_1^4} - \frac{3F_1'}{R_1^3} + \frac{F_1''}{R_1^2}\right)$$

$$\frac{\partial g}{\partial z} = \frac{z - z_i}{R_1}\left(\frac{3F_1}{R_1^4} - \frac{3F_1'}{R_1^3} + \frac{F_1''}{R_1^2}\right)$$

$$\frac{\partial u_r}{\partial t} = r\left(\frac{\partial f}{\partial t} + \frac{\partial g}{\partial t}\right)$$

$$\frac{\partial u_z}{\partial t} = z\left(\frac{\partial f}{\partial t} + \frac{\partial g}{\partial t}\right) - z_i\frac{\partial g}{\partial t} \tag{17}$$

$$\frac{\partial f}{\partial t} = -c\left(\frac{F'}{R^3} - \frac{F''}{R^2}\right)$$

$$\frac{\partial g}{\partial t} = -c\left(\frac{F'}{R_1^3} - \frac{F''}{R_1^2}\right) .$$

By the generalized Hook's law, the stress functions are readily obtained. They are

$$\sigma_r = \lambda\left(\frac{\partial u_r}{\partial r} + \frac{\partial u_z}{\partial z} + \frac{u_r}{r}\right) + 2\mu\frac{\partial u_r}{\partial r}$$

$$\sigma_z = \lambda\left(\frac{\partial u_r}{\partial r} + \frac{\partial u_z}{\partial z} + \frac{u_r}{r}\right) + 2\mu\frac{\partial u_z}{\partial z}$$

$$\sigma_\phi = \lambda\left(\frac{\partial u_r}{\partial r} + \frac{\partial u_z}{\partial z} + \frac{u_r}{r}\right) + 2\mu \cdot \frac{u_r}{r} \tag{18}$$

$$\tau_{rz} = \mu\left(\frac{\partial u_r}{\partial z} + \frac{\partial u_z}{\partial r}\right) ; \tau_{r\phi} = \tau_{\phi z} = 0 .$$

At the axis of cylindrical symmetry, $r = 0$, $\tau_{rz} = 0$ at the free surface, but τ_{rz} is nonzero off the axis on the free surface. This means that the image system in Figure 7b is not able to meet the requirement of zero stress condition on the boundary. In order to balance the shear stress on the boundary, a second fictitious system is imposed. An artificial shear stress distribution is applied externally in such a way that it equals the negative value of τ_{rz} evaluated on the free boundary (at $z = R_s$). It is known that the shear stress applied on a free boundary will propagate into the material at the speed of the shear stress wave which is slower than the dilatational wave speed (see Ref. 12). Because the spallation takes place near the free boundary, it is assumed that the applied shear stress distribution is invariant along the z-direction. Hence

$$\tilde{\tau}_{rz} = \tau_{rz} - \tau_{rz}(r, o, t) \tag{19}$$

is the "effective" shear stress.

From the relations in Equations 18 and 19, the principle stress and directions are computed:

$$\begin{aligned} p &= \frac{\sigma_r + \sigma_z}{2} + \left[\left(\frac{\sigma_r - \sigma_z}{2}\right)^2 + \tilde{\tau}_{rz}^{\,2}\right]^{\frac{1}{2}} \\ q &= \frac{\sigma_r + \sigma_z}{2} - \left[\left(\frac{\sigma_r - \sigma_z}{2}\right)^2 + \tilde{\tau}_{rz}^{\,2}\right]^{\frac{1}{2}} \\ \gamma &= \frac{1}{2}\tan^{-1}\left(\frac{2\,\tilde{\tau}_{rz}}{\sigma_r - \sigma_z}\right) \quad . \end{aligned} \tag{20}$$

RESULTS AND DISCUSSION

A sample spallation problem has been calculated based on the formulations in the previous sections. The plate thickness is chosen as 10 d, where d is the diameter of the projectile. The aluminum-on-aluminum impact is considered and the following material characteristic data are used in the calculations (Ref. 12):

- Dilatational wave speed, $c = 6.32$ km/sec
- Lame's constants: $\lambda = 0.56$ megabar
  $\mu = 0.26$ megabar.

The initial condition of the elastic wave propagation is specified by the shock solution of Reference 1, in which a rectangular cylinder impacts upon a plate at the velocity of 20 km/sec.

Figures 8, 9, and 10 show the stress distribution for different values of radial position r. The general features are the same except for the time delay. The time is measured from the point at which the wave front first reaches the free boundary. For instance, at the axis of symmetry ($r = 0$), the tensile stress of 14 kilobars occurs at a time of 6.02 microseconds and the same stress occurs at 9.54 microseconds on $r = 0.2$ d (Figure 10). In spite of the different time delays, the distances from the free surface to the point of 14 kilobars are the same for different r. The maximum stress distributions after wave reflection are plotted in Figure 11 in which the lines of the principal stress 5, 10, 14, and 20 kilobars are presented.

It is noted that the constant stress lines are essentially parallel to the free surface. If the maximum dynamic stress of aluminum is taken as 14 kilobars, the line AB in Figure 11 represents the spall fracture locus in the target material. Even though no direct comparison can be made with experimental data, the general features are compatible with the observations in References 7 and 9.

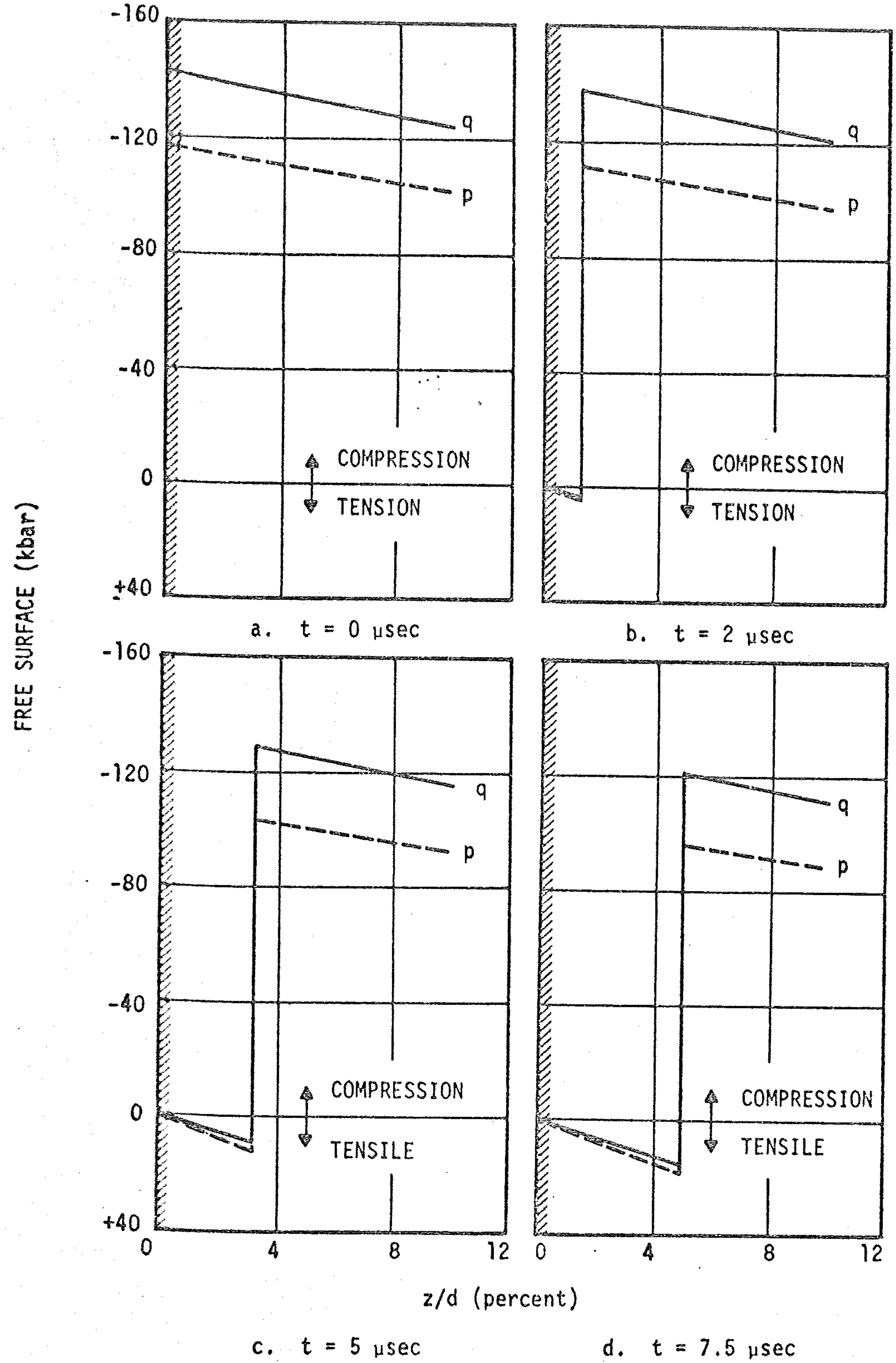

FIGURE 8. THE STRESS DISTRIBUTIONS ON THE r = 0 AXIS AT THE SUCCESSIVE TIME STEPS

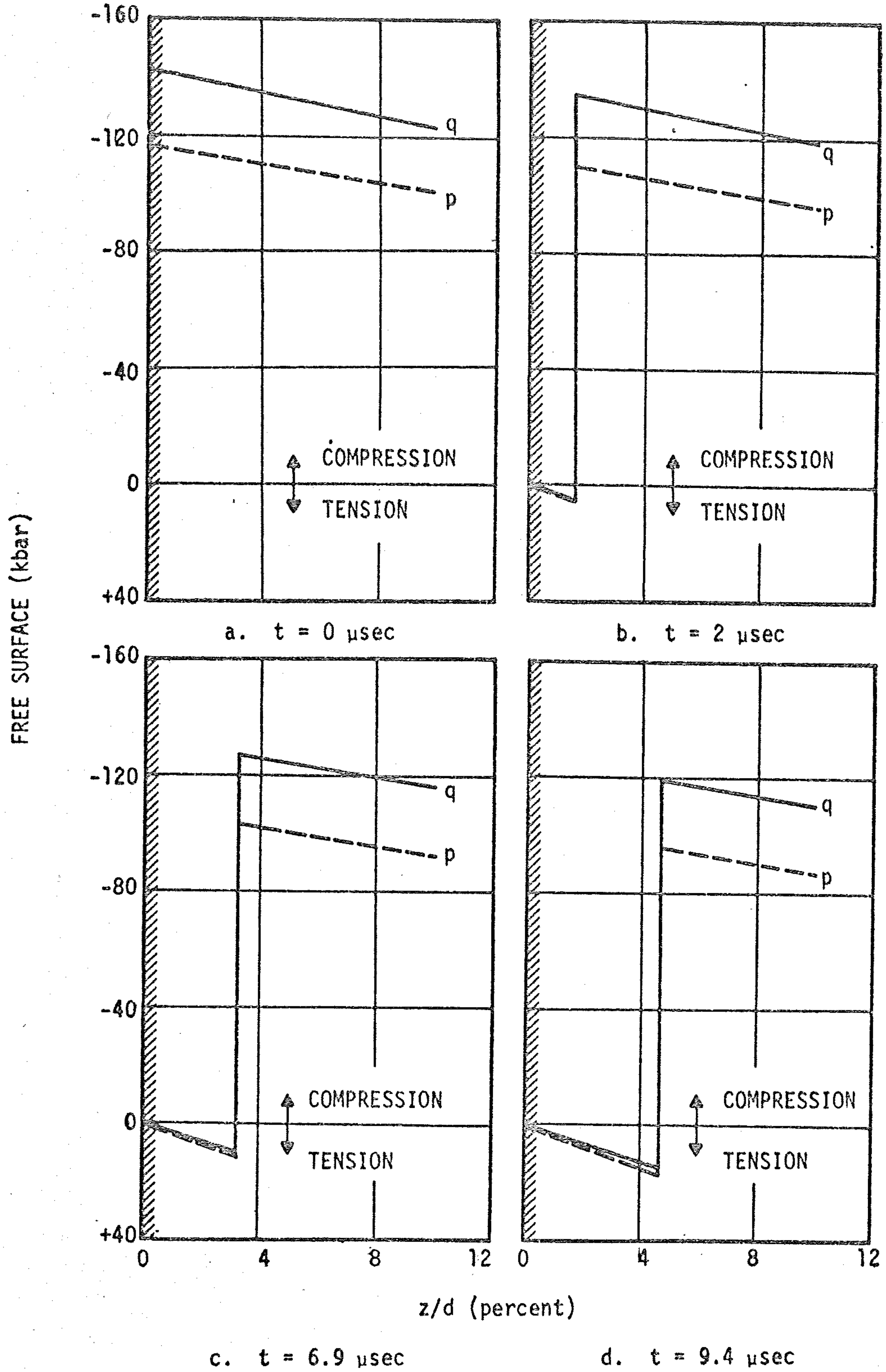

FIGURE 9. THE STRESS DISTRIBUTION ON r = 0.1 d AT THE SUCCESSIVE TIME STEPS

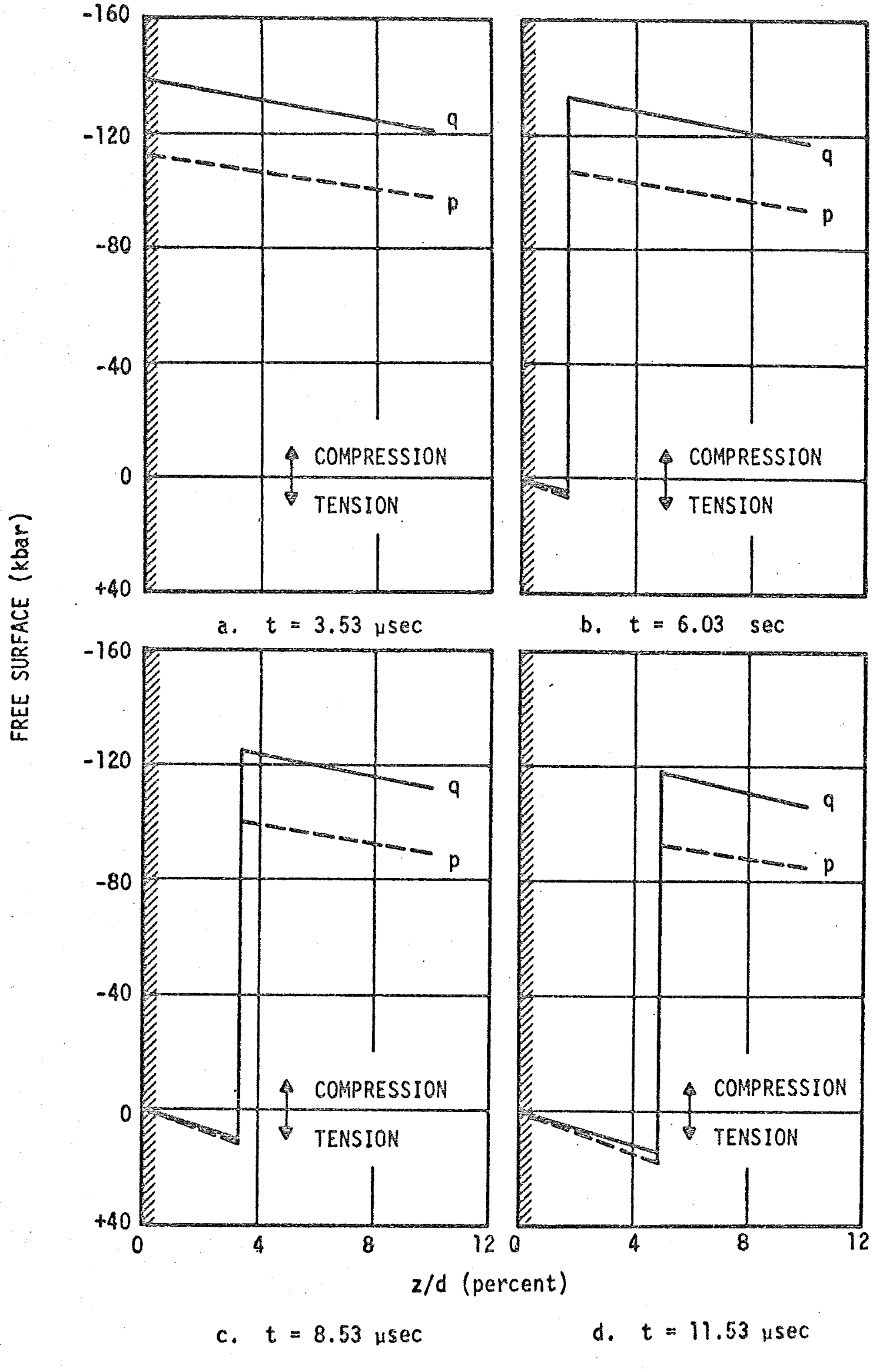

FIGURE 10. THE STRESS DISTRIBUTION ON r = 0.2 d AT THE SUCCESSIVE TIME STEPS

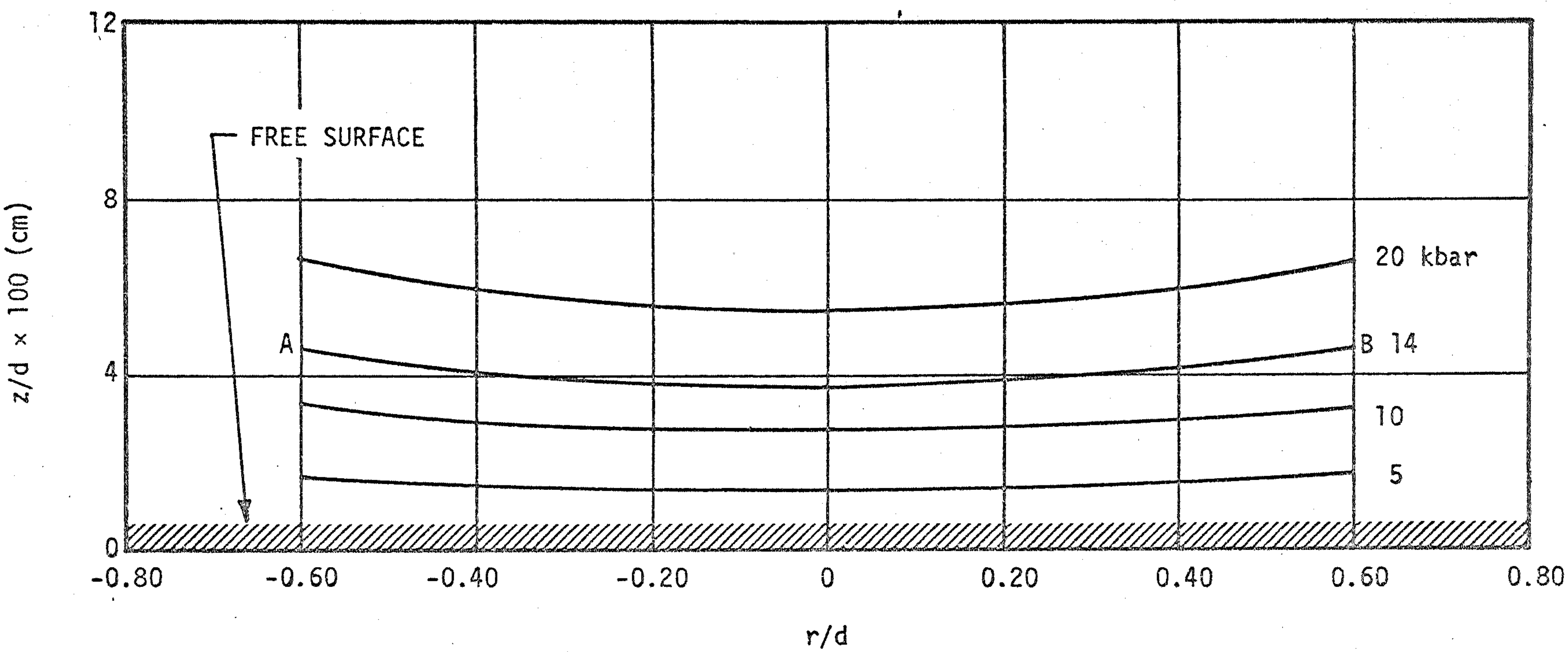

FIGURE 11. MAXIMUM STRESS DISTRIBUTION AFTER WAVE REFLECTION

REFERENCES

1. Rae, W. J., "Comments on the Solution of the Spall Fracture Problem in the Approximation of Linear Elasticity", NASA CR-54250, CAL Report AI 1821-A-3, January 1965

2. Fu, T., "Shock Propagation in a Target Subjected to Hyper-velocity Impact of an Incident Projectile", Brown Engineering Company, Inc., Technical Note SE-289, April 1970

3. Aliev, Kh. M., "Reflection of Spherical Elastic Waves at the Boundary of a Half-Space", Ahurnal Prikladnoi Mekhaniki i Teknicheskoi Friziki, No. 6, November - December 1961. Translated in FTD TT-65-994 (AD624924), November 1965

4. Rinehart, J. S., "On Fractures Caused by Explosions and Impacts", Quarterly of the Colorado School of Mines, Volume 55, No. 4, October 1960

5. Kinslow, R., "Properties of Spherical Stress Waves Produced by Hypervelocity Impact", AEDC-TDR-63-197, October 1963

6. Kinslow, R., "Observations of Hypervelocity Impact of Transparent Plastic Target", AEDC-TDR-64-49, May 1964

7. Kinslow, R., "Properties of Reflected Stress Waves", AIAA Paper No. 69-363, May 1969

8. Christman, D. R. and N. H. Froula, "Dynamic Properties of High-Purity Beryllium", AIAA Paper No. 69-360, May 1969

9. Piacesi, R. and J. W. Watt, "A Study of the Role of Mechanical-Strength Properties on the Phenomena of Spallation", U. S. Naval Ordnance Laboratory, No. 1TR 66-42, January 1966

10. Heyda, J. F. and T. D. Riney, "Penetration of Structures by Hypervelocity Projectiles", General Electric Company, Space Sciences Laboratory, Report No. R64D3, February 1964

11. Hayes, W. D. and R. F. Prostein, Hypersonic Flow Theory, Academic Press, 1959

12. Kolsky, H., Stress Waves in Solids, Oxford Press, p. 201, 1953